Supplementary Information
Regional gravitational phases and a geometric active-charge law for dark-sector phenomenology

Yuzhan Zhang

1 Supplementary Note 1: Minimal tri-stable phase field

Three locally stable scalar phases separated by barriers require at least five ordered stationary points. Hence a polynomial derivative must have degree at least five and the potential degree at least six. A convenient normalized representative is

$$W_0(\chi) = \frac{4}{3}\chi^6 - 3\chi^4 + 2\chi^2, \tag{S1}$$

with a linear unfolding $W(\chi; H) = W_0(\chi) - H\chi$. At zero bias, $\chi = 0$ is the global minimum, $\chi = \pm 1$ are metastable minima and $\chi = \pm 1/\sqrt{2}$ are barriers. Stationary points satisfy

$$8\chi^5 - 12\chi^3 + 4\chi - H = 0. \tag{S2}$$

Numerically the positive coexistence point is

$$H_{\mathrm{coex}} = 0.341688495018, \tag{S3}$$

where the central and positive minima have equal free energy and the equilibrium order parameter jumps from 0.087415890295 to 1.035423691165. The central spinodal is $H = 0.928501997833$, while the positive daughter branch persists under reverse bias to $H = -0.435940$. These constants are reproduced by `analysis_phase.py`. The numerical coefficients are a normalization; only the tri-stable catastrophe structure is used in the main argument.

2 Supplementary Note 2: Exact spherical regional-state identities

For an Einstein–de Sitter spherical overdensity,

$$R = A(1 - \cos\theta), \qquad t = B(\theta - \sin\theta), \tag{S4}$$

with

$$\frac{\rho_\Omega}{\rho_{\mathrm{bg}}} = \frac{9}{2}\frac{(\theta - \sin\theta)^2}{(1 - \cos\theta)^3}, \tag{S5}$$

$$\frac{H_\Omega}{H_{\mathrm{bg}}} = \frac{3}{2}\frac{(\theta - \sin\theta)\sin\theta}{(1 - \cos\theta)^2}. \tag{S6}$$

The regional coordinate of the main text therefore satisfies

$$\Upsilon_{\mathrm{over}} = \frac{H_\Omega/H_{\mathrm{bg}}}{\sqrt{\rho_\Omega/\rho_{\mathrm{bg}}}} = \cos(\theta/2). \tag{S7}$$

For a spherical underdensity,

$$R = A(\cosh\eta - 1), \qquad t = B(\sinh\eta - \eta), \tag{S8}$$

and

$$\frac{\rho_\Omega}{\rho_{\rm bg}} = \frac{9}{2}\frac{(\sinh\eta-\eta)^2}{(\cosh\eta-1)^3}, \tag{S9}$$

$$\frac{H_\Omega}{H_{\rm bg}} = \frac{3}{2}\frac{(\sinh\eta-\eta)\sinh\eta}{(\cosh\eta-1)^2}, \tag{S10}$$

so that

$$\Upsilon_{\rm void} = \cosh(\eta/2). \tag{S11}$$

The linearly extrapolated underdensity is

$$\delta_L = -\frac{3}{5}\left[\frac{3}{4}(\sinh\eta-\eta)\right]^{2/3}. \tag{S12}$$

Matter–curvature equality is $\Upsilon = \sqrt{2}$, hence $\eta = 2\,\mathrm{arcosh}\,\sqrt{2}$, and yields

$$\delta_{L,*} = -0.516745404162, \qquad \rho_\Omega/\rho_{\rm bg} = 0.638816488503. \tag{S13}$$

Mature spherical void shell crossing at $\delta_L = -2.717$ instead gives $\Upsilon \simeq 2.94672$ and $\rho/\bar{\rho} \simeq 0.205$.

3 Supplementary Note 3: First-passage and power-spectrum timing audit

The provisional phase-conversion bookkeeping uses a Brownian excursion between a positive collapse barrier $\delta_c = 1.686$ and a negative V-phase barrier δ_v. Following the standard two-barrier void bookkeeping [2, 3], for shifted coordinate $0 < y < L$, the absorbing heat kernel is

$$p(y,\tau) = \frac{2}{L}\sum_{n=1}^{\infty}\sin\frac{n\pi y_0}{L}\sin\frac{n\pi y}{L}\exp\left[-\frac{n^2\pi^2\tau}{2L^2}\right]. \tag{S14}$$

Boundary fluxes give the cumulative first-passage fractions. The shell-crossing choice $\delta_v = -2.717$ requires

$$\tau_{1/2} = 2.940769839691 \tag{S15}$$

for the chosen half-volume Eulerian landmark. With Planck-like $\sigma_8 = 0.811$ and standard transfer shapes, the variance on $R_L \sim 9-11\,h^{-1}$Mpc is much smaller, so this selector is excluded as a viable abundance mechanism within the stated prototype. Replacing the late barrier by matter–curvature equality gives

$$\tau_{1/2} = 0.358216707503, \tag{S16}$$

which lies in the variance range of large-void Lagrangian scales. This is an external consistency audit, not a self-consistent background solution.

4 Supplementary Note 4: Basin antichain and history-dependent occupation

Let $\mathcal{T}$ be a laminar watershed or merge-tree hierarchy [4]. A set of eligible nodes $E \subset \mathcal{T}$ is reduced to its maximal elements under inclusion,

$$\mathcal{V} = \max_{\subseteq} E. \tag{S17}$$

Proposition 1. *$\mathcal{V}$ is an antichain.*

If two selected nodes were nested, the smaller would have an eligible strict ancestor and would not be maximal, a contradiction. Thus the active union can be represented without nested double counting.

For first-order hysteresis the instantaneous eligibility and actual phase occupation are distinct. In the strongest absorbing limit,

$$\mathcal{A}_V(t_{n+1}) = \mathcal{A}_V(t_n) \cup \mathcal{E}_V(t_{n+1}), \tag{S18}$$

followed by maximal-node reduction. A deterministic hierarchy stress test in `analysis_basin_dynamics.py` produces fewer state switches than an instantaneous classifier and a monotone active-union filling fraction, as expected.

5 Supplementary Note 5: Conversion sign and interface coarsening

If a V phase with fixed internal energy density $\varepsilon_V > 0$ irreversibly occupies a monotonically increasing fraction $\phi_V(a)$, then $\bar{\rho}_V = \varepsilon_V \phi_V$. Re-expressing the total dark sector as conserved dust plus a residual component gives

$$w_{\mathrm{res}}(a) = -\frac{a^3 \phi_V(a)}{3\int_0^a a'^2 \phi_V(a')\mathrm{d}a'} \le -1, \tag{S19}$$

where the inequality follows from monotonicity of ϕ_V. Thus irreversible bulk filling with negligible interfaces cannot generate present-day $w > -1$.

Positive interface energy changes the conclusion. Let

$$s_\Sigma = A_\Sigma/V, \qquad L_\Sigma = 3\phi_V/s_\Sigma, \qquad \ell_\Sigma = \sigma_\Sigma/\varepsilon_V. \tag{S20}$$

Then

$$\rho_{V+\Sigma} = \varepsilon_V \phi_V \left(1 + 3\ell_\Sigma/L_\Sigma\right). \tag{S21}$$

Differentiating the conservation equation gives the exact condition

$$w_{\mathrm{app}} > -1 \quad \Longleftrightarrow \quad \frac{\mathrm{d}\ln L_\Sigma}{\mathrm{d}\ln a} > \left(1 + \frac{L_\Sigma}{3\ell_\Sigma}\right)\frac{\mathrm{d}\ln \phi_V}{\mathrm{d}\ln a}. \tag{S22}$$

Coarsening can therefore move the effective residual from phantom-like back through -1 without assigning an intrinsic $w(a)$ to the bulk phase.

6 Supplementary Note 6: Diffuse-interface and thin-wall constants

For the phase-field functional

$$\mathcal{F} = \int \left[\frac{\kappa}{2}|\nabla\chi|^2 + \mathcal{E}_0(W - W_{\min})\right]\mathrm{d}^3x, \tag{S23}$$

the planar coexistence wall obeys

$$\frac{\kappa}{2}(\partial_z\chi)^2 = \mathcal{E}_0(W - W_{\min}). \tag{S24}$$

Numerical quadrature for the normalized sextic gives

$$\sigma_\Sigma = 0.396830116706\sqrt{\kappa\mathcal{E}_0}, \qquad d_{10-90} = 1.693129938128\sqrt{\kappa/\mathcal{E}_0}. \tag{S25}$$

Writing $\xi_0 = \sqrt{\kappa/\mathcal{E}_0}$, a thin-wall daughter domain with bulk advantage Δf has

$$R_c = \frac{2\sigma_\Sigma}{\Delta f}. \tag{S26}$$

If the dimensionless bulk free-energy difference is matched linearly to Hamiltonian imbalance,

$$\Delta w_V = \beta_\Gamma(\Gamma - 1), \tag{S27}$$

then

$$\frac{R_c}{\xi_0} = \frac{2C_\sigma}{\beta_\Gamma(\Gamma-1)}, \qquad \Gamma_{\rm grow}(R) = 1 + \frac{2C_\sigma}{\beta_\Gamma}\frac{\xi_0}{R}. \tag{S28}$$

The relation reduces an arbitrary bias function to a normalization and a correlation length, but neither is derived microscopically.

7 Supplementary Note 7: Proof of the geometric active-charge theorem

Let Φ_b be the baryonic potential, S_ϕ a closed equipotential leaf, and $\psi = f(\Phi_b)$. With $\alpha = f'(\phi)$, $|\nabla\psi| = \alpha g_b$. Define

$$I_1(\phi) = \int_{S_\phi} g_b \mathrm{d}A = 4\pi G M_b, \qquad I_2(\phi) = \int_{S_\phi} g_b^2 \mathrm{d}A. \tag{S29}$$

The coarea formula reduces

$$\mathcal{I}_3 = \frac{1}{12\pi G a_E}\int \alpha^3 I_2 \mathrm{d}\phi + \int f(\phi)\frac{\mathrm{d}M_b}{\mathrm{d}\phi}\mathrm{d}\phi. \tag{S30}$$

The Euler–Lagrange equation is

$$\frac{\mathrm{d}}{\mathrm{d}\phi}\left(\frac{I_2\alpha^2}{4\pi G a_E}\right) = \frac{\mathrm{d}M_b}{\mathrm{d}\phi}. \tag{S31}$$

Regularity at the innermost leaf sets the integration constant to zero, so

$$I_2\alpha^2 = 4\pi G a_E M_b. \tag{S32}$$

The emergent active charge is

$$Q_e = \frac{1}{4\pi G}\int_{S_\phi} |\nabla\psi| \mathrm{d}A = \alpha M_b. \tag{S33}$$

Hence

$$Q_e^2 = \frac{4\pi G a_E M_b^3}{I_2}. \tag{S34}$$

With $M_A = a_E A/(4\pi G)$ and

$$\eta_S = \frac{I_1^2}{A I_2} = \frac{\langle g_b\rangle_S^2}{\langle g_b^2\rangle_S}, \tag{S35}$$

one obtains

$$Q_e^2 = \eta_S M_b M_A. \tag{S36}$$

Cauchy–Schwarz gives $I_1^2 \le A I_2$, therefore $0 < \eta_S \le 1$, with equality for constant g_b on the leaf.

8 Supplementary Note 8: Three-dimensional synthetic basin stress test

This test is deliberately constructed as an obstruction rather than as an N-body surrogate. Four periodic Gaussian fields are generated in a $256\,h^{-1}$Mpc box on an 80^3 grid, with power shape $P(k) \propto k^{0.9665}T^2(k)$, normalized so that a top-hat at $8\,h^{-1}$Mpc has rms 0.811. Each field is smoothed at $4\,h^{-1}$Mpc, then segmented into non-spherical watershed basins. Marker persistence is varied over 0, 0.05, 0.10 and 0.20 times the smoothed-field rms.

For each basin, the voxel volume defines $R_{\rm eff}$, and the regional mean linear underdensity is mapped through the exact spherical-void relation to Γ. The conditional finite-size criterion uses $\xi_0 = 3.12938\,h^{-1}$Mpc and $\beta_\Gamma = 1$. Across the four seeds, the zero-persistence fraction satisfying $\Gamma \ge 1$ is $3.14\% - 5.35\%$, while the stricter finite-size-active fraction is only $1.70\% - 2.94\%$. Across all persistence settings, the latter spans 0.67% − 2.94%. Thus a single-scale instantaneous Gaussian watershed does not generate a volume-dominant V phase. The result specifically motivates nonlinear basin evolution, hierarchy/history or a different coarse-graining rule.

All numbers above are reproduced by `analysis_synthetic_3d_basins.py`; the power normalization is verified to machine precision for each seed.

9 Supplementary Note 9: History-dependent Zel'dovich basin stress test

The static Gaussian watershed test in Supplementary Note 8 contains no dynamical history. We therefore perform a second, still deliberately limited, three-dimensional test in which the watershed basins are defined in Lagrangian space and followed through a Zel'dovich deformation. The purpose is to determine whether the minimal quasi-linear history missing from the static test is already sufficient to generate a large V-phase filling fraction.

The linearly extrapolated smoothed density field obeys $\nabla^2\Phi = \delta_L$, and the mapping is

$$\mathbf{x}(\mathbf{q}, D) = \mathbf{q} - D\nabla\Phi(\mathbf{q}). \tag{S37}$$

If λ_i are the local eigenvalues of the Hessian of Φ, the deformation Jacobian is

$$J = \prod_i (1 - D\lambda_i). \tag{S38}$$

For a fixed Lagrangian basin with initial coordinate volume V_L, its Eulerian coordinate volume and regional density are

$$V_E(D) = \int_\Omega J\, \mathrm{d}^3 q, \qquad \frac{\bar{\rho}_\Omega}{\bar{\rho}_{\rm bg}} = \frac{V_L}{V_E}. \tag{S39}$$

In the Einstein–de Sitter timing convention, $D = a$, differentiation of the physical basin volume $a^3 V_E$ gives

$$\frac{H_\Omega^{\rm loc}}{H_{\rm bg}} = 1 + \frac{D}{3V_E}\frac{\mathrm{d}V_E}{\mathrm{d}D}. \tag{S40}$$

These two quantities determine Υ_Ω and hence $\Gamma_\Omega = \Upsilon_\Omega^2 - 1$ without mapping the mean basin density through a spherical model. First shell crossing is identified by $D\lambda_{\max} \geq 1$. The strict V-phase test requires the full Lagrangian basin to remain pre-shell-crossing, to have positive regional expansion, and to satisfy the same conditional finite-size inequality used in the main text. We also report a kinematic upper envelope in which the basin-wide single-stream requirement is dropped; this deliberately estimates how much of the low abundance can be blamed on the strict shell-crossing cut.

Four fixed Gaussian realizations and three watershed persistence choices are followed at $D = 0.25, 0.50, 0.75, 1.00$. The Fourier Hessian trace reproduces the smoothed density field with maximum error 1.78×10^{-15}, and the periodic Zel'dovich volume closes to unity within 4.8×10^{-6} over the frozen grid. At $D = 1$, the strict instantaneous finite-size-active Eulerian fraction spans

$$0.002614 \leq \phi_{V,\rm inst} \leq 0.038907. \tag{S41}$$

If activation is treated as absorbing along each fixed basin history, the final range is

$$0.007302 \leq \phi_{V,\rm hist} \leq 0.048485. \tag{S42}$$

The kinematic upper envelope, which ignores the basin-wide single-stream condition, remains only

$$0.014988 \leq \phi_{V,\rm kin} \leq 0.087218. \tag{S43}$$

Thus the low filling fraction is not solely a consequence of the strict single-stream criterion. Minimal quasi-linear history raises the active fraction but still fails to produce a volume-dominant V phase.

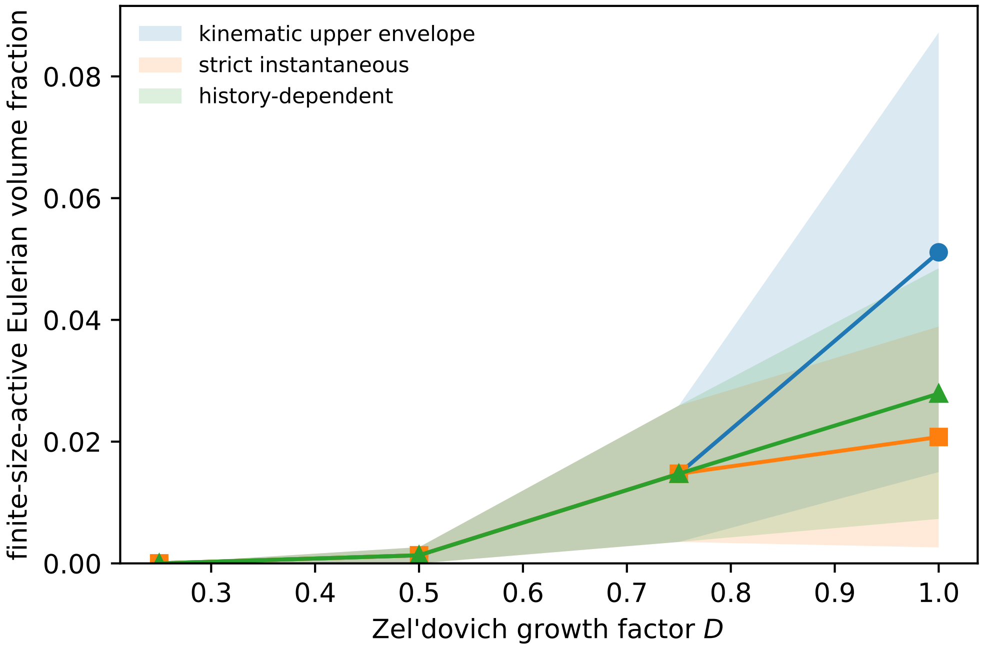

Figure S1: History-dependent Zel'dovich stress test. Bands show the extrema across the frozen seed/persistence grid. The absorbing history lies above the strict instantaneous classifier but remains far below a volume-dominant expanding phase. The kinematic upper envelope remains below 9% at $D = 1$.

This calculation should not be read as an N-body void catalogue. The Zel'dovich approximation is valuable precisely because it captures the onset of anisotropic deformation, caustics and multistream structure while remaining analytically transparent, but it does not describe the full nonlinear hierarchy and merger dynamics of the late cosmic web. Published N-body watershed studies track long-lived void identities, annexed subvoids and merger histories that are absent from the present fixed-Lagrangian-basin construction. The negative result therefore narrows the next calculation to nonlinear basin hierarchy and history rather than validating or excluding the broader regional-phase hypothesis.

All values are reproduced by `analysis_zeldovich_basin_history.py`.

10 Supplementary Note 10: SPARC diagnostic details

The galaxy consistency check uses the public SPARC radial-acceleration table [7, 8] with 2,693 points from 175 disk galaxies. The spherical finite-amplitude relation is

$$g = \frac{1}{2}\left(g_b + \sqrt{g_b^2 + 4a_E g_b}\right). \tag{S44}$$

Only a_E is optimized. Quoted uncertainty in both logarithmic axes is propagated approximately as

$$\sigma_i^2 = \sigma_{y,i}^2 + \left(\frac{\partial \log_{10} g_{\mathrm{model}}}{\partial \log_{10} g_b}\right)^2 \sigma_{x,i}^2. \tag{S45}$$

The deterministic result is

$$a_E = 1.097458984856508 \times 10^{-10}\ \mathrm{m\,s^{-2}}, \quad \chi^2/\mathrm{dof} = 1.610215393925522, \tag{S46}$$

with raw rms 0.132909757608 dex. This does not refit distance, inclination or stellar mass-to-light ratios and is not a model-selection likelihood.

11 Supplementary Methods: Reproducibility inventory

The GitHub-ready release contains deterministic scripts for the phase potential, spherical regional state, first-passage fractions, power-spectrum clock, curvature selector, basin-antichain logic, conversion sign theorem, history-dependent basin occupation, interface coarsening, diffuse-wall constants, thin-wall fronts, Hamiltonian-bias matching, galaxy diagnostic, three-dimensional synthetic basin test and history-dependent Zel'dovich basin test. Regression tests freeze all numerical constants used in the manuscript. The reproducibility package for this submission is designated GitHub release `v1.2.0` (`https://github.com/Wujijiandao/ainstein-regional-dark-phases/releases/tag/v1.2.0`) and is archived under the stable project DOI `https://doi.org/10.5281/zenodo.22042564`. The public GitHub-safe archive fetches SPARC data from the source rather than redistributing the third-party table; the self-contained archival package can be supplied privately to editors and referees if required.

12 Supplementary References

References

[1] Eisenstein, D. J. & Hu, W. Baryonic features in the matter transfer function. *Astrophys. J.* **496**, 605–614 (1998). doi:10.1086/305424.

[2] Sheth, R. K. & van de Weygaert, R. A hierarchy of voids: much ado about nothing. *Mon. Not. R. Astron. Soc.* **350**, 517–538 (2004). doi:10.1111/j.1365-2966.2004.07661.x.

[3] Jennings, E., Li, Y. & Hu, W. The abundance of voids and the excursion set formalism. *Mon. Not. R. Astron. Soc.* **434**, 2167–2181 (2013). doi:10.1093/mnras/stt1169.

[4] Sousbie, T. The persistent cosmic web and its filamentary structure – I. Theory and implementation. *Mon. Not. R. Astron. Soc.* **414**, 350–383 (2011). doi:10.1111/j.1365-2966.2011.18394.x.

[5] Hidding, J., Shandarin, S. F. & van de Weygaert, R. The Zel'dovich approximation: key to understanding cosmic web complexity. *Mon. Not. R. Astron. Soc.* **437**, 3442–3472 (2014). doi:10.1093/mnras/stt2142.

[6] Sutter, P. M. et al. The life and death of cosmic voids. *Mon. Not. R. Astron. Soc.* **445**, 1235–1244 (2014). doi:10.1093/mnras/stu1845.

[7] Lelli, F., McGaugh, S. S. & Schombert, J. M. SPARC: mass models for 175 disk galaxies with Spitzer photometry and accurate rotation curves. *Astron. J.* **152**, 157 (2016). doi:10.3847/0004-6256/152/6/157.

[8] McGaugh, S. S., Lelli, F. & Schombert, J. M. Radial acceleration relation in rotationally supported galaxies. *Phys. Rev. Lett.* **117**, 201101 (2016). doi:10.1103/PhysRevLett.117.201101.